Shear wave profiles from surface wave inversion: the impact of uncertainty on seismic site response analysis

2011 J. Geophys. Eng. 8 162

(http://iopscience.iop.org/1742-2140/8/2/004)

IOP Publishing Journal of Geophysics and Engineering
J. Geophys. Eng. **8** (2011) 162–174 doi:10.1088/1742-2132/8/2/004

Shear wave profiles from surface wave inversion: the impact of uncertainty on seismic site response analysis

J Boaga[1], **G Vignoli**[1,2] **and G Cassiani**[1]

[1] Dipartimento di Geoscienze, Università degli Studi di Padova, Padova, Italy
[2] Earth Sciences Department, King Fahd University of Petroleum & Minerals, Dhahran, Saudi Arabia

E-mail: jacopo.boaga@unipd.it

Received 8 April 2010
Accepted for publication 10 January 2011
Published 10 March 2011
Online at stacks.iop.org/JGE/8/162

Abstract
Inversion is a critical step in all geophysical techniques, and is generally fraught with ill-posedness. In the case of seismic surface wave studies, the inverse problem can lead to different equivalent subsoil models and consequently to different local seismic response analyses. This can have a large impact on an earthquake engineering design. In this paper, we discuss the consequences of non-uniqueness of surface wave inversion on seismic responses, with both numerical and experimental data. Our goal is to evaluate the consequences on common seismic response analysis in the case of different impedance contrast conditions. We verify the implications of inversion uncertainty, and consequently of data information content, on realistic local site responses. A stochastic process is used to generate a set of 1D shear wave velocity profiles from several specific subsurface models. All these profiles are characterized as being equivalent, i.e. their responses, in terms of a dispersion curve, are compatible with the uncertainty in the same surface wave data. The generated 1D shear velocity models are then subjected to a conventional one-dimensional seismic ground response analysis using a realistic input motion. While recent analyses claim that the consequences of surface wave inversion uncertainties are very limited, our test points out that a relationship exists between inversion confidence and seismic responses in different subsoils. In the case of regular and relatively smooth increase of shear wave velocities with depth, as is usual in sedimentary plains, our results show that the choice of a specific model among equivalent solutions strongly influences the seismic response. On the other hand, when the shallow subsoil is characterized by a strong impedance contrast (thus revealing a characteristic soil resonance period), as is common in the presence of a shallow bedrock, equivalent solutions provide practically the same seismic amplification, especially in the frequency range of engineering interest.

Keywords: surface waves, inversion, seismic site response, soil resonance period

1. Introduction

In situ shear wave surveys are geophysical tools of usual practice in earthquake engineering. 1D models of shear wave velocity profiles are obtained using several techniques, from borehole investigation to classical SH reflection prospecting, or surface wave dispersion analyses. In traditional engineering surveys, borehole techniques have been considered as standard, due to their relative reliability (Moss 2008), even though they are relatively expensive and not very suitable for the very critical situation of intensely urbanized settings. Recently, surveys based on surface wave dispersion analysis have been intensely developed, leading to a number of affordable methodologies. These approaches are in fact free from many practical and theoretical limitations of body-wave analyses and from the logistic effort of drilling. In addition, the

surface wave approach is favoured by the fact that Rayleigh and Love waves dominate every seismogram, because of the two-dimensional geometric spreading that reduces their attenuation with distance and the prevalent generation of surface waves when using surface sources.

Surface wave dispersion is linked to subsoil characteristics as different frequencies involve different soil thicknesses, and consequently travel at different velocities (Knopoff 1972). Dispersion properties can be measured by several procedures, based on phase velocities (e.g. MASW (Park *et al* 1999), SASW (Nazarian *et al* 1983), REMI (Louie 2001, Strobbia and Cassiani 2010)) and on group velocities (e.g. FTAN (Levshin *et al* 1972, Nunziata *et al* 1999)). A further distinction is made between controlled source surveys and passive analysis of microtremors and seismic noise (see Pritchett (1989), Zywicki and Rix (1999), Wathelet (2005), Rosenblad and Li (2009), Lobkis and Weaver (2001)).

Different approaches to describe and handle surface wave propagation in non-1D media have been described and investigated in the literature (Keilis-Borok *et al* 1989, Abraham *et al* 2004, Strobbia and Foti 2006, Socco *et al* 2008, Strobbia *et al* 2009, Vignoli and Cassiani 2009, Vignoli *et al* 2010), but today's practice is mostly limited to the inversion of data in terms of 1D shear velocity profiles. Density and Poisson ratios are generally fixed *a priori*, since surface wave dispersion is almost insensitive to these parameters (Socco and Strobbia 2004). The goodness of this simplification has been discussed in several parametric studies about Rayleigh wave propagation in layered media (Nazarian 1984). Moreover, this is the reason why it is usual practice to present the results of dispersion curve inversion as shear wave velocity profiles.

Irrespective of the specific approach adopted, the solution of the inverse problem still represents one of the critical points of the surface wave techniques, due to its ill-posedness. The presence of errors in the data inevitably propagates from the data to the model space: in the case of data collected with active seismic sources, as in MASW, these errors are more severe in the low-frequency range, and the associated uncertainty propagates specifically to affect the deepest levels of the shear wave profile (Lai and Wilmanski 2005).

Non-uniqueness and instability are particularly severe in the inversion of surface wave dispersion curves (Cercato 2009), also because of the strong nonlinearity of the problem. A usual strategy to overcome this ill-posedness is to reduce the dimension of the model space, for example by using a very simplified parameterization (e.g. a 1D stack of very few homogeneous horizontal isotropic layers) or sophisticated regularization techniques (Zhdanov 2002, Huang *et al* 2003). Looking for a (regularized) inversion solution means to select the desired (stable) solution from the class of solutions, i.e. the class of all models compatible with the data within the noise level (with specific physical and/or geometrical properties). Applications of stabilizers other than the traditional smoothers is relatively scarce in the surface wave literature (Lai and Wilmanski 2005, Trampert and Spetzler 2006, Strobbia *et al* 2009) even though successful applications have been reported for other geophysical methods (Zhdanov and Tolstaya 2004, Zhdanov *et al* 2006, Vignoli and Zanzi 2006, Pagliara and Vignoli 2006). The use of few homogeneous layers sometimes leads to oversimplified solutions, but, in practice, all methods add to the inversion some degree of *a priori* information (e.g. on smoothness) that may or may not correspond to reality. In all cases, data inversion faces the uncertainty of the measurement process that is ultimately projected onto the model space. Solutions can be selected among all models fitting the data within their estimated accuracy range, and this can also be achieved by an extensive exploration of the model space by Monte Carlo approaches (e.g. Socco and Boiero (2008)) that provide a better evaluation of the data information content. In particular in the case of shear wave profiles, the choice of the optimal solution has substantial consequences in terms of practical engineering demands, as earthquake local amplification depends strongly on the existing shear velocity profile of the near subsurface.

The influence of the near-surface condition on ground shaking has been taken into account in earthquake engineering studies for many years, albeit in a simplified manner. The most common approach to evaluate the contribution of subsoil properties to seismic motion is the theoretical ground responses analysis (Aki 1970, Seed 1969, Bard 1995). Surface motion amplification is a direct consequence of the conservation of elastic wave energy, since S-wave velocities and densities are smaller near the surface than at greater depth. This implies the fundamental role of a shallow subsurface material, even though seismic waves may travel through kilometres of rigid crust and less than 100 m of soft soil.

Transfer functions are generally used to describe the relationship between earthquake input motion at the base of the soil column and the resulting surface ground shaking. This approach is based on the principle of superposition and consists in analysing a nonlinear system by an iterative study of approximating equivalent linear soils. This is the case of the most used 1D analyses, involving soil deposit layers of different stiffness and damping characteristics with boundaries in which elastic wave energy is reflected and/or transmitted. These synthetic ground motion analyses develop transfer functions for layered soil characterized by specific values of shear modulus, damping and density (Idriss and Seed 1969). The most widely used code for this purpose is SHAKE (Schnabel *et al* 1972, Idriss and Sun 1992), which implements a linear equivalent analysis based on continuous layer discretization in the frequency domain. It is worth noting that the linear equivalent approach does not consider the influence of surface topography (Chavez-Garcia *et al* 1997) nor other 2D or 3D effects (Bard and Bouchon 1985).

The key objective of this study is to analyse the impact of uncertainty of surface wave inversion on the consequent evaluation of earthquake amplitude amplification. The aim of our work is not to focus on the uncertainties of the inversion procedure itself, but rather to emphasize the consequences of these uncertainties on standard seismic response analysis. In fact, uncertainty consequences are particularly important in special subsoil conditions. Recently, Foti *et al* (2008) concluded that the consequences of surface wave inversion uncertainties are very limited in terms of seismic responses, but their analysis is focused on considering only certain types

Table 1. Bottom half-space shear wave velocities of the five considered synthetic cases.

Case	Bottom half-space S-wave velocity
A	320 m s^{-1}
B	500 m s^{-1}
C	700 m s^{-1}
D	900 m s^{-1}
E	1000 m s^{-1}

of shallow subsoil structures that present a sharp impedance contrast (about 2.5) in the shallow subsoil. In this paper, we want to extend the analysis to a wider range of cases, considering in particular alluvial plain cases characterized by deep seismic bedrock often unreachable by common surveys. Our ultimate goal is to draw guidelines assessing in which cases more accurate knowledge of the shallow subsurface S-wave structure is needed, in contrast to cases where even an approximate knowledge is sufficient for shaking prediction. In particular, as the usual 1D shaking analysis is mainly controlled by impedance contrasts between the soil layers, we seek criteria based on such impedance contrasts.

2. Synthetic cases

The purpose of our synthetic analysis is to explore how shaking prediction of different subsurface structures may suffer from the propagation of surface wave inversion uncertainty. We define five different 1D reference models (A, B, C, D, E—see figures 1(*a*), 3(*a*), 5(*a*), 7(*a*), 9(*a*), pink lines). As the impedance contrast between soil and bedrock is one of the expected key factors, we built up the five models mentioned above with gradually different impedance contrasts. These models are characterized by increasing value of the shear wave velocities of the bottom half-space. In this work, we consider cases with slow increase of elastic soil parameters in depth (without a strong acoustic impedance contrast), and cases characterized by well-defined seismic bedrocks (e.g. having $V_s > 700$ m s^{-1} at the bottom of the profile). The five starting models were chosen to identify different subsoil conditions, from usual plain environment to shallow bedrock conditions. We increased progressively in five steps the shear wave velocity of the bottom half-space from 320 to 1000 m s^{-1} (table 1). Poisson ratio and density values are the same in all layers of all five models (soil density = 2000 kg m^{-3}, Poisson ratio = 0.33), because of the negligible impact that these parameters have on Rayleigh wave dispersion curves. 2000 kg m^{-3} is a rough approximation: by excess, for a soil comprising mainly clay, silt and fine sand, and, by defect, for a soil containing a large portion of stone, gravel and coarse sand (Keefe 2005). We chose 0.33 for the Poisson ratio as an approximation corresponding to a large variety of soils (Coduto 2001). Even reasonable values very different from those for the density and Poisson ratio would not affect the results significantly (Nazarian 1984, Socco and Strobbia 2004).

For each of the five considered starting models we calculated the theoretical dispersion curves (figures 1(*b*), 3(*b*), 5(*b*), 7(*b*), 9(*b*), pink line) using a forward model based on Dunkin's (1965) formalism and Wathelet's (2005) suggestions.

Table 2. Layer thickness and shear wave velocity standard deviations used to define the subset of the model space to be stochastically sampled.

	Layer thickness st. dev.	Shear wave velocity st. dev.
1st layer	2 m	5 m s^{-1}
2nd layer	10 m	25 m s^{-1}
3rd layer	20 m	50 m s^{-1}
4th layer	30 m	75 m s^{-1}
Half-space		100 m s^{-1}

Then, we specified a neighbourhood of this theoretical curve simulating the uncertainty of real measurements (Lai *et al* 2005). The upper (figures 1(*b*), 3(*b*), 5(*b*), 7(*b*), 9(*b*), solid red line) and lower (figures 1(*b*), 3(*b*), 5(*b*), 7(*b*), 9(*b*), solid blue line) curves delimiting the neighbourhood have been defined by adding to the calculated reference dispersion curve (figures 1(*b*), 3(*b*), 5(*b*), 7(*b*), 9(*b*), pink line), for every frequency, a quantity, $\pm\Delta V_R = \pm(0.05 V_R + 100/f)$, directly proportional to velocity and inversely proportional to frequency. The proportionality coefficients are respectively 0.05 and 100 m s^{-2}. The same coefficients were used for all models. The choice of these coefficients is arbitrary, but it guarantees that the uncertainty bounds of the dispersion curves are falling within the usual uncertainty of this kind of measurement as reported in the literature (Lai *et al* 2005). The choice of this expression for the quantity ΔV_R defining the limits of the admissible dispersion curve neighbourhood takes into account the behaviour of the uncertainty with respect to frequency and velocity. Indeed, the uncertainty of the phase velocity, $V_R = 2\pi f/k$, can be evaluated considering a first-order approximation as $\sigma_{V_R} = \left|V_R^2/(2\pi f)\right| \sigma_k$. Thus, a higher degree of uncertainty is expected in the low-frequency range and for high velocity (Strobbia and Foti 2006).

After that, we stochastically sample a subset of the model space about the starting model. Each subset is defined by the Gaussian distribution of the parameters (layer thickness and S-wave velocity) with means equal to the parameter value of the specific starting model (figures 1(*a*), 3(*a*), 5(*a*), 7(*a*) and 9(*a*), pink lines). For all cases (A, B, C, D and E) the standard deviations for each Gaussian distribution have been chosen according to table 2. Thickness and velocity standard deviations in table 2 are the same for all the models and, albeit *arbitrarily*, they are chosen to account for the increase of uncertainty with depth. We generate random models from the above distributions, and we consider the first 50 models (figures 1(*a*), 3(*a*), 5(*a*), 7(*a*) and 9(*a*), black lines) corresponding to the dispersion curves (figures 1(*b*), 3(*b*), 5(*b*), 7(*b*) and 9(*b*), black lines) lying within the neighbourhood of the starting model curve as described above. The (pseudo-)random numbers used to generate the random models are obtained by means of the Mersenne twister algorithm (Matsumoto and Nishimura 1998) as it is implemented in the commercial numerical computing environment Matlab. This procedure (and this choice of

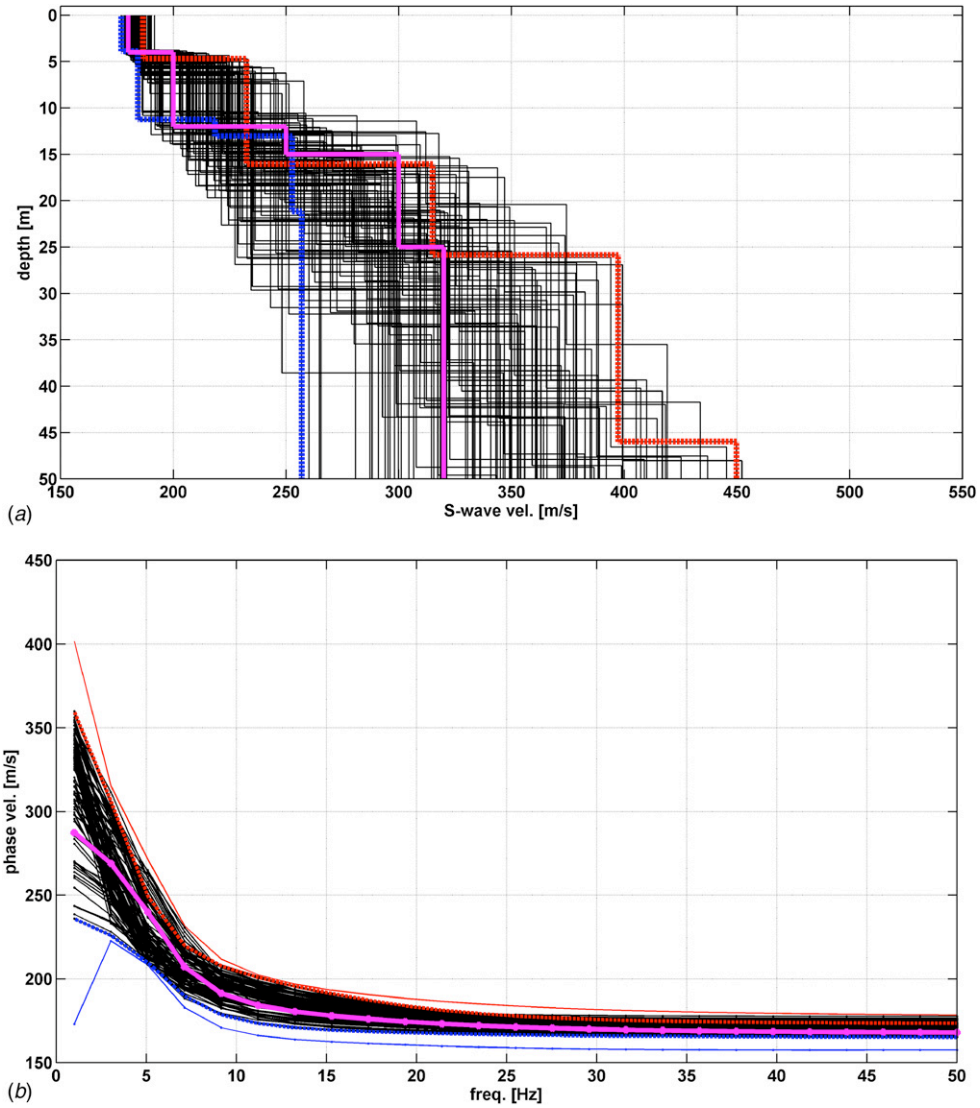

Figure 1. (*a*) The pink line shows the 1D shear wave velocity profile chosen as the starting structure for case A. The black solid lines show the selected models having equivalent dispersion curves and belonging to the possible solution subset. The blue and red lines represent the selected profiles closest to the accuracy limits as in (*b*). (*b*) The thick pink (light grey) line shows the theoretical dispersion curve for the starting structure in (*a*). The black lines are the curves corresponding to the structures sampled from the subset of possible models. The dotted, red and blue, lines show the curves closest to the boundaries of the accuracy neighbourhood (solid, red and blue, lines).

the parameter defining the Gaussian) guarantees a very large model variability, but, at the same time, avoids instability problems: in principle, even a curve very close to the starting dispersion curve can correspond to a model too far from the starting model. We can interpret the criterion for defining the sampled model space subset as the *a priori* information we have about the solution, i.e. it corresponds to our regularization approach. The selected solutions have to face not only the data, but also the prior information we have about the physical system we are investigating. We pick up the solutions among all models compatible with the data and close enough to what we know is the true model.

In summary, we generated a dataset composed of 250 synthetic models from five starting shear velocity profiles.

All the generated models were tested using the common horizontal layer seismic responses code SHAKE91 (Idriss and Sun 1992). As input motion at the base of the soil columns, we selected a strong seismic episode of the 1976 Friuli earthquake

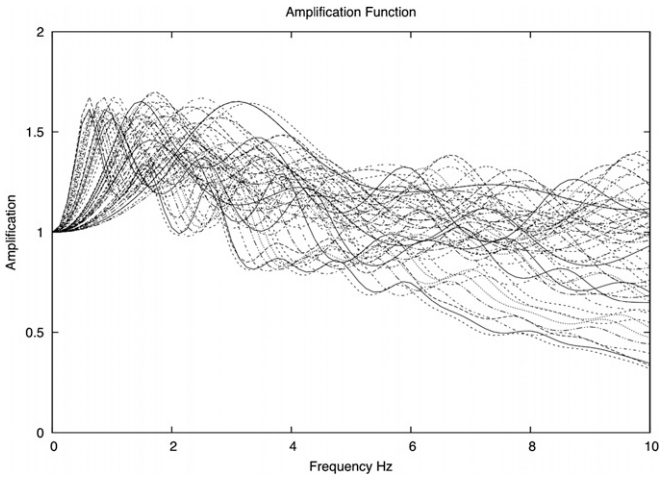

Figure 2. Synthetic elastic analysis amplification spectra from the S-wave profiles obtained for case A.

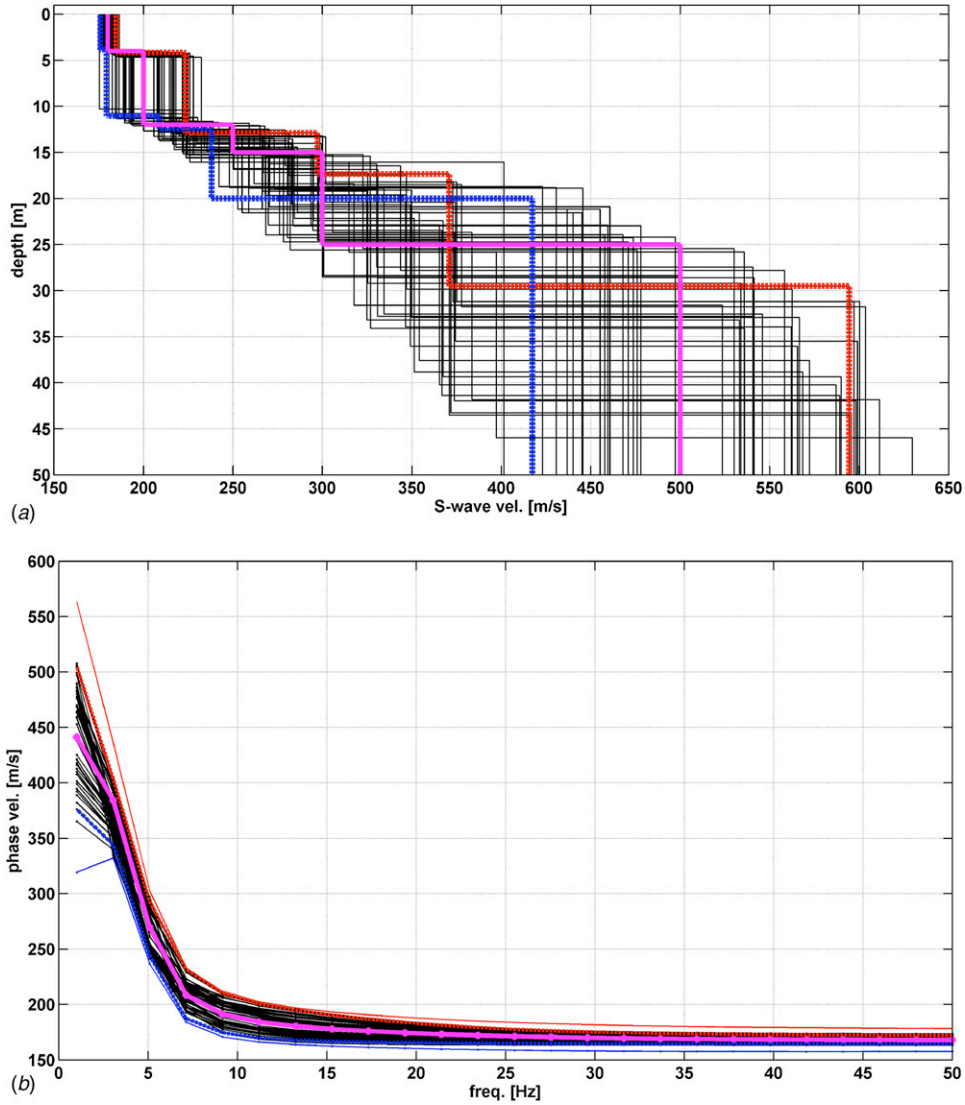

Figure 3. (*a*) The pink line shows the velocity profile chosen as the starting structure for case B; the model is equal to model A, but for the bottom half-space velocity (now 500 m s^{-1}). The black solid lines show the selected models having equivalent dispersion curves; in particular, the red and blue lines represent those closer to the accuracy limits as in (*b*). (*b*) The thick pink (light grey) line shows the theoretical dispersion curve for the starting structure of (*a*). The black lines are the curves corresponding to the structures sampled from the subset of possible models. The dotted, red and blue, lines show the curves closest to the boundaries of the 'accuracy' neighbourhood (solid, red and blue, lines).

(the biggest one recorded in Northeastern Italy, $Ms = 6.5$), recorded 50 km from the epicentre on a stiff outcrop. In order to select a relationship connecting damping and shear waves modulus, we resorted to the literature values (Idriss 1990, Seed and Idriss 1970, Seed *et al* 1986) compatible with the selected subsoil characteristics (table 3).

The first model (model A) is a subsoil profile which presents a smooth increase of velocities with depth. It has four layers (thickness: 4, 8, 3 and 10 m) with velocities 180, 200, 250 and 300 m s^{-1}, respectively, over a half-space with V of 320 m s^{-1}. As a result of the shaking simulation, the seismic amplification spectra show very notable differences. In such subsoil conditions, very common in deep alluvial plains, the selected uncertainties of the inversion problem lead to seismic motion scenarios that are significantly different. The computed amplification spectra, obtained using the same seismic input, show very similar amplification peaks in terms

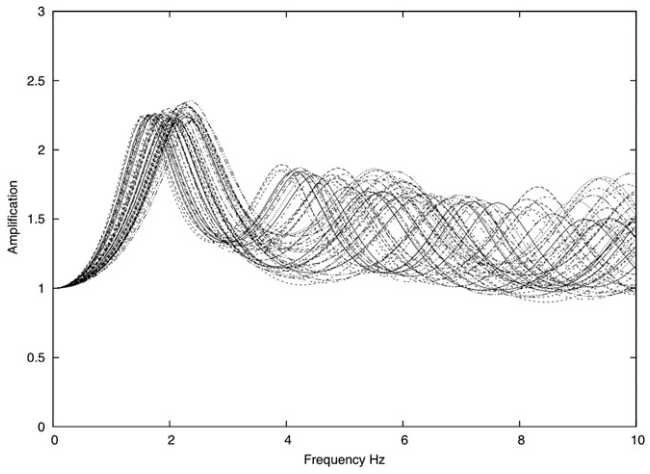

Figure 4. Synthetic elastic analysis amplification spectra for case B.

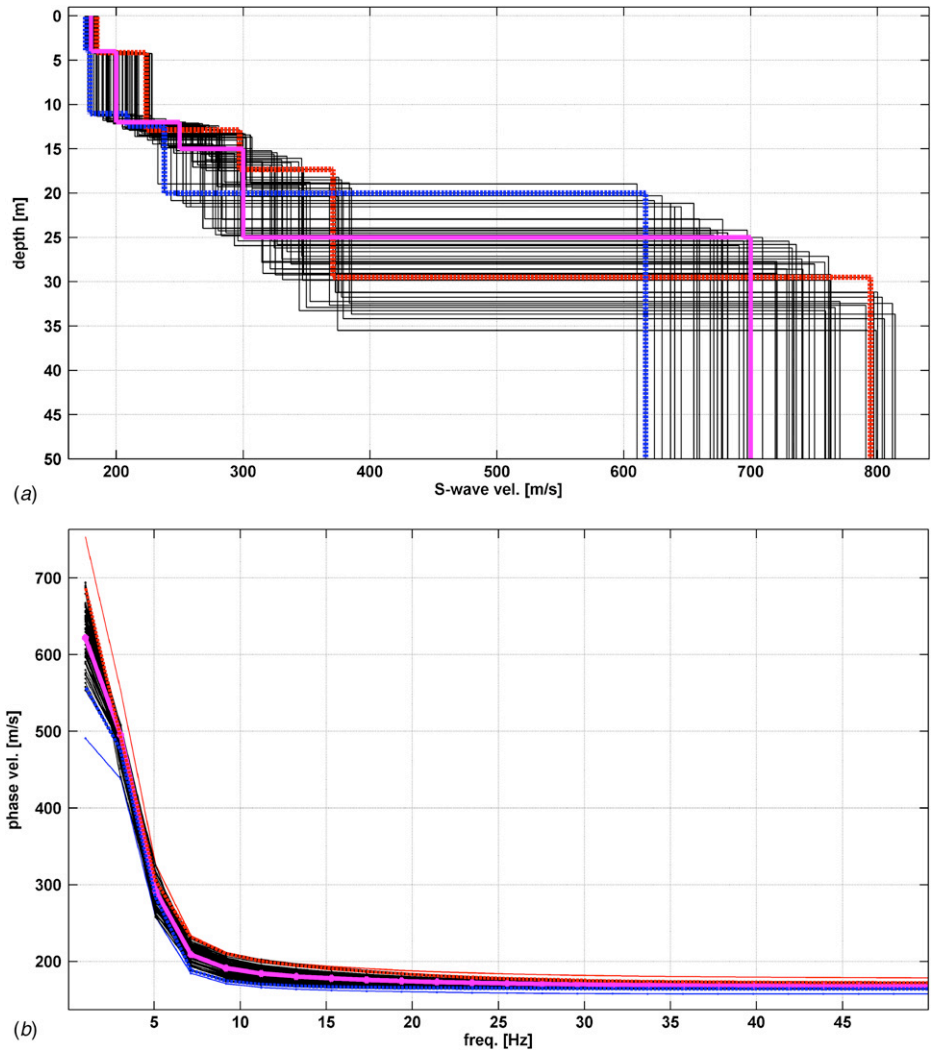

Figure 5. (*a*) The pink line shows the velocity profile chosen as the starting structure for case C; the model is equal to model A, but for the bottom half-space velocity (now 700 m s^{-1}). The black solid lines show the selected models having equivalent dispersion curves; in particular, the red and blue lines represent those closer to the accuracy limits as in (*b*). (*b*) The thick pink (light grey) line shows the theoretical dispersion curve for the starting structure of (*a*). The black lines are the curves corresponding to the structures sampled from the subset of possible models. The dotted, red and blue, lines show the curves closest to the boundaries of the 'accuracy' neighbourhood (solid, red and blue, lines).

of amplitude (see figure 2) but very different in terms of peak frequency. In the frequency range of typical engineering interest, the peak frequency varies from 0.5 to 3.3 Hz. This implies that for conditions similar to those of case A, different acceptable surface wave inverse solutions lead to significantly different earthquake designs.

In case B, the bottom of the starting model has a higher velocity, $V_s = 500$ m s^{-1} (figure 3(*a*)). The equivalent solution profiles were shaken with the same seismic input as that of case A. In this test, the amplification spectra derived from all the possible inversion solutions reveal again a large difference in terms of the frequencies excited by seismic motion (figure 3(*b*)). Moreover, as expected, the absolute amplification peaks are larger in amplitude than those in case A. Once again, the maximum amplification frequencies present a significant variation from 1.4 to 2.5 Hz (figure 4).

In synthetic case C, the velocity V_s of the deepest layer is raised to 700 m s^{-1} (figure 5(*a*)). In this case the amplification

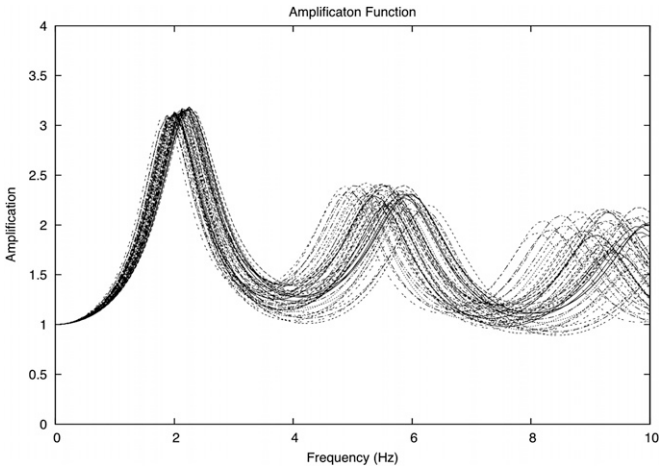

Figure 6. Synthetic elastic analysis amplification spectra for case C.

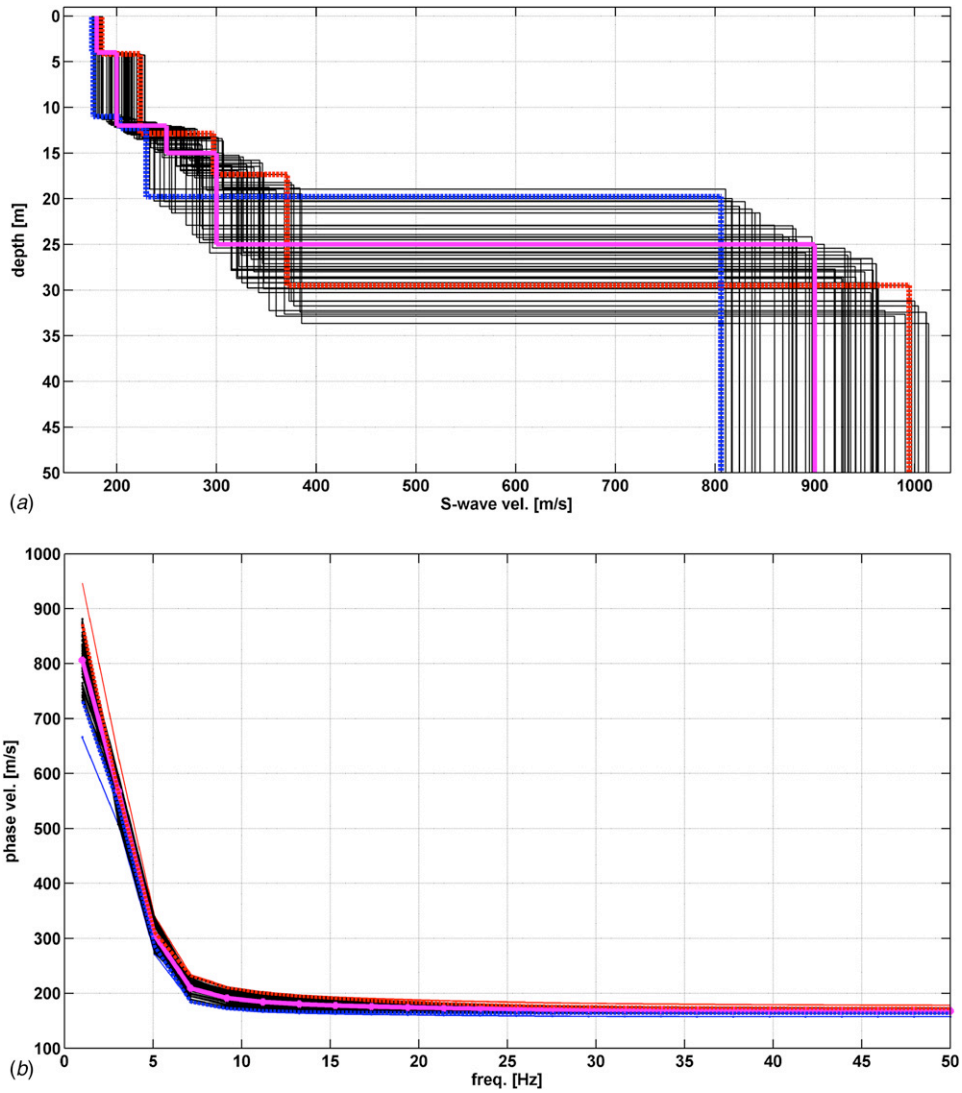

Figure 7. (*a*) The pink line shows the velocity profile chosen as the starting structure for case D; the model is equal to model A, but for the bottom half-space velocity (now 900 m s^{-1}). The black solid lines show the selected models having equivalent dispersion curves; in particular, the red and blue lines represent those closer to the accuracy limits as in (*b*). (*b*) The thick pink (light grey) line shows the theoretical dispersion curve for the starting structure of (*a*). The black lines are the curves corresponding to the structures sampled from the subset of possible models. The dotted, red and blue, lines show the curves closest to the boundaries of the 'accuracy' neighbourhood (solid, red and blue, lines).

spectra, computed with the same seismic input, present a similar ground seismic response for the fundamental frequency of vibration, while have a significant difference for higher modes (figure 6).

When the synthetic model has a bedrock with very high velocity ($V_s = 900$ m s^{-1}—case D), the seismic responses are practically unaffected by the inversion solution uncertainties. Figure 8 shows that all the acceptable equivalent solutions (figure 7(*b*)) provide similar seismic ground motions. In this case, the non-uniqueness of the inversion does not lead to different seismic scenarios, making the result insensitive to the choice of one specific solution within the set of the acceptable solutions (figure 7(*a*)).

Finally, the synthetic case E considers a starting structure with a bottom half-space having a 1000 m s^{-1} shear wave velocity (figure 9(*a*)). The amplification spectra of the accepted solutions are practically the same for all acceptable

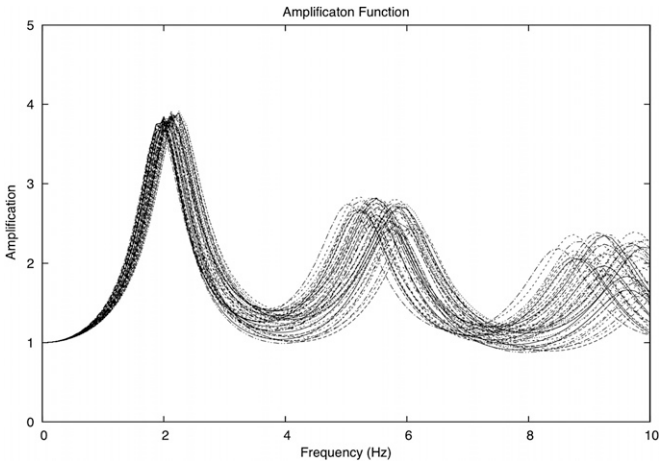

Figure 8. Synthetic elastic analysis amplification spectra for case D.

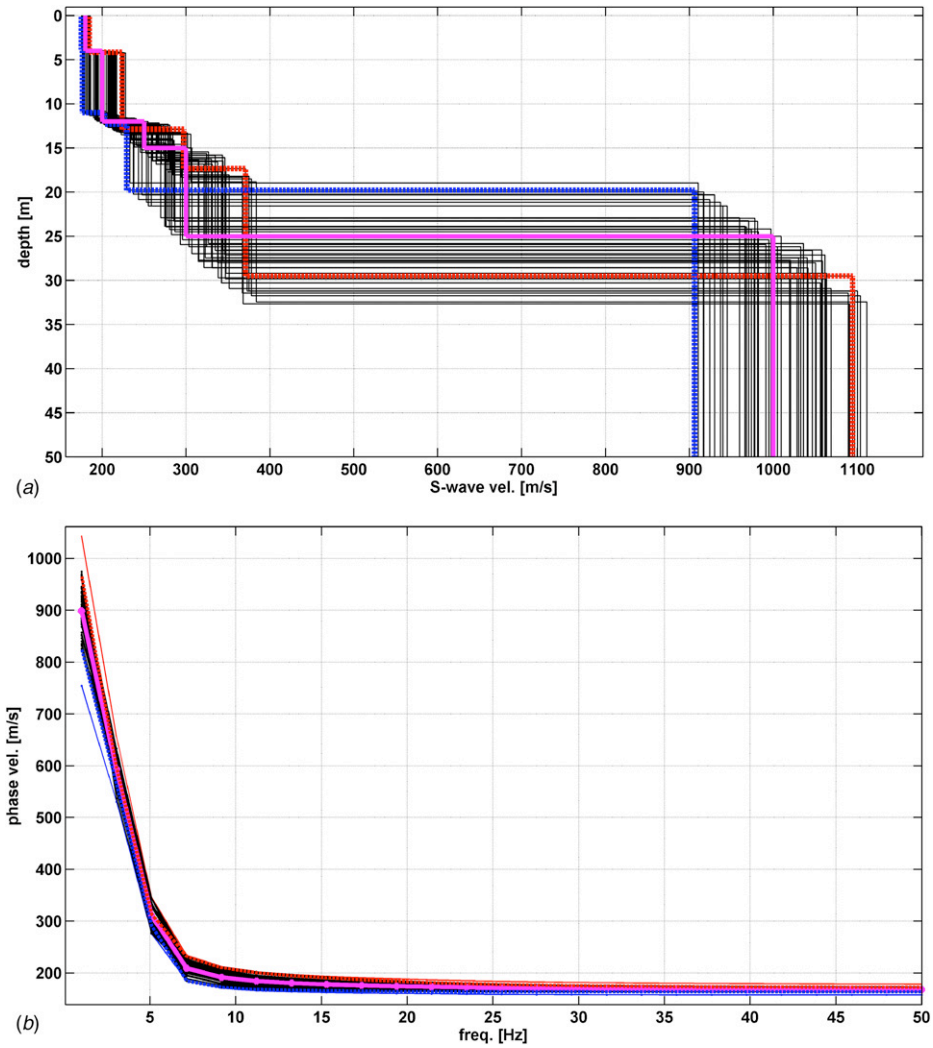

Figure 9. (*a*) The pink line shows the velocity profile chosen as the starting structure for case E; the model is equal to model A, but for the bottom half-space velocity (now 1000 m s^{-1}). The black solid lines show the selected models having equivalent dispersion curves; in particular, the red and blue lines represent those closer to the accuracy limits as in (*b*). (*b*) The thick pink (light grey) line shows the theoretical dispersion curve for the starting structure of (*a*). The black lines are the curves corresponding to the structures sampled from the subset of possible models. The dotted, red and blue, lines show the curves closest to the boundaries of the 'accuracy' neighbourhood (solid, red and blue, lines).

inversion solutions. This confirms that, in this case, the effects of the model uncertainties propagating to seismic responses are negligible (figure 10).

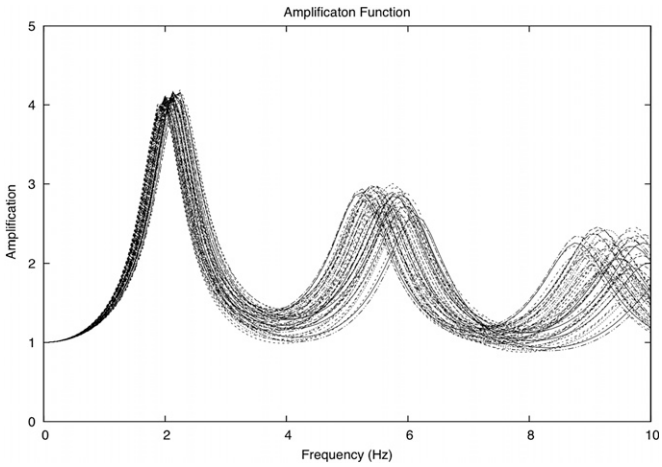

Figure 10. Synthetic elastic analysis amplification spectra for case E.

3. Real case test

We also consider a case of real experimental data. In order to verify the effective consequences of model uncertainties, we performed a surface wave acquisition at a site located in the pre-alpine plain of Northeast Italy (figure 11). A multi-channel analysis of surface wave (MASW) (Park *et al* 2007) experiment was conducted using a setup of 24 vertical geophones with a 4.5 Hz natural frequency. Starting from the experimental dispersion curve, to study the neighbourhood of the model solution, we adopted the same strategy as for the synthetic cases. Thus, first, we performed a deterministic inversion of the observed curve using the approach discussed, for example, in Vignoli and Cassiani (2009). In this way, we retrieved the model in figure 12(*a*) (pink line) from the experimentally

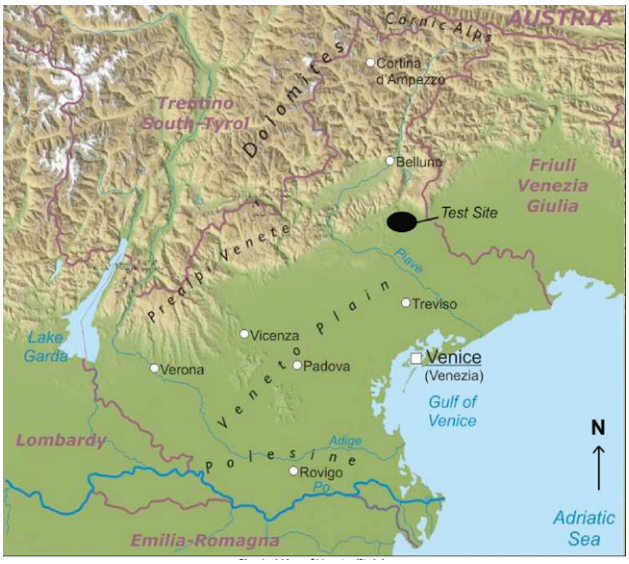

Figure 11. Test site location in Northeastern Italy.

observed dispersion curve in figure 12(*b*) (pink line). Such a model is used as the reference model to perform the statistical analysis. Then, we defined the subset of the model space to be sampled by means of the Gaussian distributions centred on the found reference model and with standard deviations as given in table 2. We estimated the data uncertainty by adding $\pm\Delta V_R$ as it was calculated for the synthetic cases. We selected as acceptable shear wave velocity profiles those with dispersion curves compatible with these data uncertainties. Figure 12(*b*) shows the acceptable dispersion curves, and figure 12(*a*) shows the corresponding V_s profiles.

The velocity profiles were then shaken with the same seismic input as that selected in the synthetic cases. As shown in figure 13, the seismic site amplification spectra are significantly heterogeneous, especially in terms of fundamental frequency variation. This result is consistent with our expectations, since the considered real case is a subsoil without a defined seismic bedrock: as in similar synthetic cases, the choice of the inversion solutions leads to very different seismic scenarios.

4. Surface wave inversion uncertainty and impedance contrast

The five reference cases discussed in section 2 show a progressive increment of the bottom velocity. This allows us to compare ground seismic behaviour and acoustic impedance contrasts. The five synthetic starting models present growing acoustic impedance contrasts: from 1.1 (case A) to 3.3 (case E). For each case, we compute the amplification peak amplitude for all the randomly generated equivalent models. We also compute the coefficient of variation of the peak frequencies ($C_v = \sigma/\mu$, where σ is the standard deviation and μ is the mean of the peak frequencies in each amplification curve ensemble) to estimate the seismic response uncertainty. Figure 14 shows the dependence of the peak frequency coefficient of variation (for the fundamental mode) on the impedance contrast between the bedrock and the overlying soil layer for the five synthetic cases (dots). The calculated points are fitted by an exponential function, defined as $C_v = 1.134\ \mathrm{e}^{-0.8549 I_c}$ where I_c is the impedance contrast (solid line).

The purpose of this paper is also to provide practical indications about the confidence level to be reached in surface wave surveys for seismic hazard evaluation. Hence, we consider the usual engineering demand for the amplification peak localization; in practical applications, the peak period has to be identified with a precision of 0.05 s (Lai *et al* 2005). According to our inversion results, this level of confidence is not reached in two out of the five considered cases. For cases A and B (small impedance contrast), σ is 0.91 and 0.43 Hz, while μ is respectively equal to 1.99 and 2 Hz. Thus, for these models, the peak frequency variation $0.5[1/(\mu-\sigma) - 1/(\mu+\sigma)] = \sigma/(\mu^2-\sigma^2)$ is larger than $\mu^2/20$ Hz (i.e. 0.05 s).

Table 3. Values of modulus reduction ($G/G_{\max}$) and damping (%) for the layers considered in SHAKE analysis.

	Strain values (%)										
	0.0001	0.0003	0.0010	0.0030	0.0100	0.0300	0.1000	0.3000	1.0000	3.0000	10.0000
1st layer											
Modulus of reduction $G/G_{\max}$	1.0000	1.0000	1.0000	0.9810	0.9410	0.8470	0.6560	0.4380	0.2380	0.1440	0.1100
Damping (%)	0.2400	0.4200	0.8000	1.4000	2.8000	5.1000	9.8000	15.5000	21.0000	25.0000	28.0000
2nd layer											
Modulus of reduction $G/G_{\max}$	1.0000	1.0000	0.9900	0.9400	0.8500	0.6400	0.3700	0.1800	0.0800	0.0440	0.0340
Damping (%)	0.2400	0.4200	0.8000	1.4000	2.8000	5.1000	9.8000	15.5000	21.0000	25.0000	28.0000
3rd layer											
Modulus of reduction $G/G_{\max}$	1.0000	0.9600	0.9700	0.7200	0.5500	0.3700	0.2000	0.1100	0.0500	0.0300	0.0300
Damping (%)	0.3200	1.0000	1.7000	2.8700	5.4200	9.5100	15.4400	20.3800	24.4700	26.7400	28.0000
4th layer											
Modulus of reduction $G/G_{\max}$	1.0000	0.9600	0.9700	0.7000	0.5400	0.3600	0.1900	0.1000	0.0500	0.0300	0.0300
Damping (%)	0.3200	1.0000	1.7000	2.8700	5.4200	9.5100	15.4400	20.3800	24.4700	26.7400	28.0000

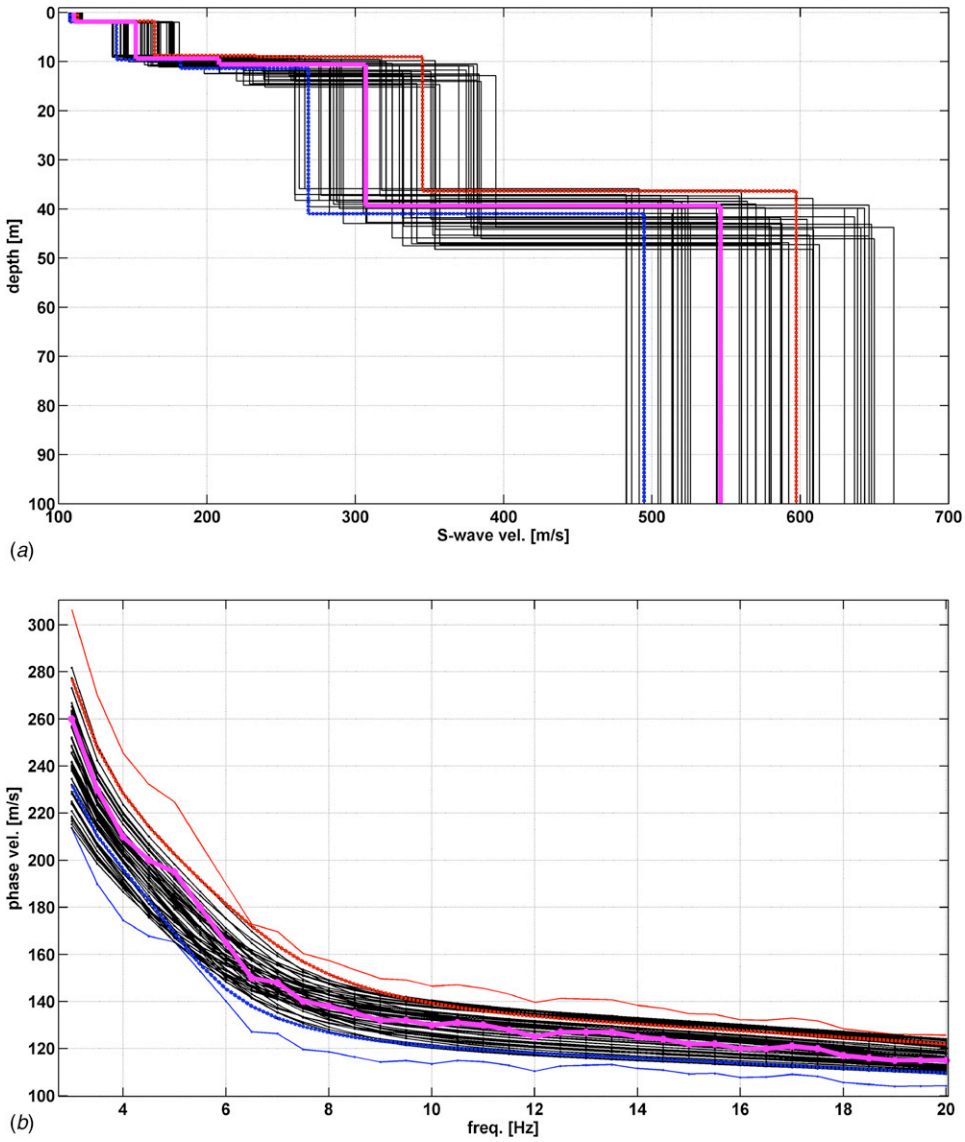

Figure 12. (*a*) The pink line is the velocity profile solution of deterministic inversion of the experimentally observed curve as in (*b*). The black solid lines show the selected models having equivalent dispersion curves. The dotted, red and blue, lines are the models with the dispersion curves closest to the boundaries of the accuracy neighbourhood. (*b*) Dispersion curves for the experimental case. In pink (light grey) is the measured dispersion curve; in red and blue (solid lines) are the limits of the accuracy neighbourhood. The dotted lines are the sampled curves closest to the limits.

On the other hand, for cases C, D and E (impedance contrast greater than 2.5) all the amplification responses reveal a precise vibration frequency, satisfying the 0.05 s accuracy range, and so, also the required earthquake design demand. In practical terms, this means that the uncertainty of the data (including the precision of the extracted dispersion curve) should be made smaller anytime a bedrock cannot be clearly identified. Note that the 2.5 value for the impedance contrast is also recognized as the limit for a defined period of vibration of a horizontally layered subsoil, as Konno and Omachi (1998) demonstrated by using synthetic and real tests; in a multi-layered system with an impedance contrast greater than 2.5, vertically incident S waves and Rayleigh waves present the same resonance period. It is known (Mucciarelli *et al* 2004) that, when a strong impedance contrast is present in the shallow subsoil within a few tens of metres from the surface, this contrast becomes the main parameter affecting

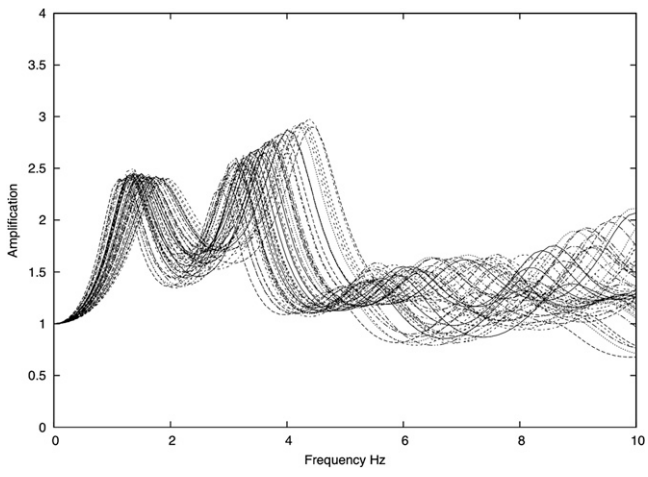

Figure 13. Synthetic elastic analysis amplification spectra for the real case.

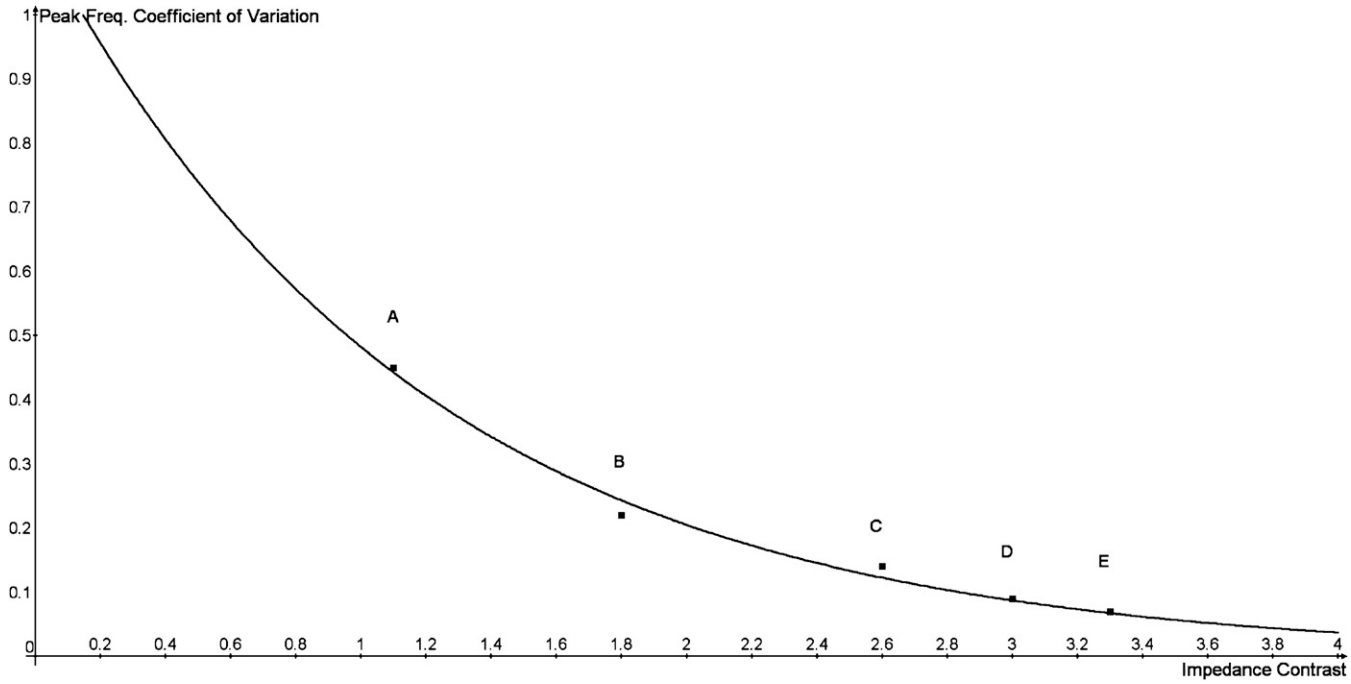

Figure 14. Variation coefficient (C_v) of the peak frequency (for the fundamental mode) versus the impedance contrast between the bottom and the overlying layer. Dots A, B, C, D and E represent the five synthetic cases of table 1.

both the frequency band of the seismic motion and the local amplification. Our results show that this subsoil parameter plays a fundamental role also in terms of the impact that surface wave inversion uncertainty has on earthquake amplification predictions.

5. Discussion

Our analysis shows, using both synthetic and real cases, that the evaluation of site seismic amplification can be very sensitive to the reliability of the S-wave inversion results. When the subsoil presents a slow change (generally, increase) of mechanical properties with depth, with no sharp contrast of acoustic impedance, the accuracy of a reconstructed S-wave velocity profile becomes an essential factor for the estimation of local seismic hazard. The absence of an abrupt change of mechanical characteristics is very common in plain sedimentation environments, which are often very urbanized and inhabited areas. These very vulnerable areas for earthquake risk are also the ones where the local shear wave velocity profile shall be known with more certainty.

In contrast, when there is a sharp acoustic impedance contrast in the shallow subsoil (i.e. there is a well-identified bedrock), different soil profiles derived from inversion of surface wave data converge to give equivalent site amplification responses. This happens because in the presence of a sharp impedance contrast what matters in terms of soil amplification is the resonant frequency of the soil layer resting upon the stiffer bedrock. This resonant frequency can be easily computed as $f_{\text{resonant}} = 4H/V_s$, where H is the soil thickness and V_s is the (average) S-wave velocity of the soil layer. This resonant frequency value is insensitive to the true values of the S-wave velocity in the bedrock underneath the impedance contrast. In the presence of a strong acoustic impedance profile, the fundamental resonance frequency does not depend on the S-wave velocity of the deeper layers, and this fact explains why in the presence of the strong impedance contrast the uncertainty in surface wave inversion does not impact the estimated resonant frequency (compare figures 2 and 10). In these particular conditions, the consequences of inversion uncertainty propagation are negligible.

In this work, we also discuss the transition between the extreme conditions just described, i.e. a well-defined bedrock and no bedrock. Figure 14 shows how the uncertainty in resonant frequency identification decreases with increasing value of the bedrock-to-soil impedance contrast. We calculated the variation coefficient of the peak frequencies (C_v) versus impedance constant (I_c) for each of the five considered synthetic cases (A, B, C, D, E in table 1). The exponential interpolation results give $C_v = 1.134\ \mathrm{e}^{-0.8549 I_c}$ revealing that a higher impedance contrast allows for a clearer identification of the resonance frequencies.

Our synthetic datasets reveal that small impedance contrast profiles present a large variation coefficient of the peak frequency. In fact, in the synthetic cases A and B (low impedance contrast), the identification of a resonant period with an accuracy larger than 0.05 s is not possible, while a smaller uncertainty is obtained for the synthetic cases C, D and E characterized by an impedance contrast greater than 2.5. This value is determined by the needed precision with which the soil resonant frequency must be known to ensure a reliable engineering design.

6. Conclusions

The non-uniqueness of solutions in geophysical inverse problems, together with the observed data noise, can play a fundamental role for the final purpose of prospecting. In the case of seismic ground motion scenarios, shear wave velocity models are the primary input for the computation of site ground response amplification. The propagation of uncertainties from the extracted dispersion curves to inversion solutions can ultimately lead to significant differences in engineering structure designs.

The analysis conducted in this study is limited to a 1D soil structure, and the amplification computations are conducted by using a simplified (albeit standard) linear equivalent approach. In spite of these limitations, the study is capable of capturing the essence of the inversion uncertainty propagation into the amplification predictions. Our work reveals that inversion accuracy has serious consequences on seismic responses under certain conditions. If no sharp impedance contrast is present in the shallow subsoil, inversion solutions require a higher accuracy, particularly in the reconstruction of the velocity values of the deepest layers. In contrast, in the presence of a strong impedance contrast (e.g. a shallow bedrock), the true value of the shear wave velocity of this bedrock is irrelevant for a reliable engineering design.

Acknowledgments

The authors wish to thank Claudio Strobbia and Rita Deiana for useful discussions. They wish to acknowledge partial funding from the University of Padova (Project 'Integration of surface wave inversion and P-wave tomography for the computation of static corrections in reflection seismics') and from the Cariparo Foundation (Excellence Project 'Transport phenomena in hydrological catchments: hydrological and geophysical experiments and modelling') that made this study possible.

References

Abraham O, Chammas R, Cote P, Pedersen H and Semblat J F 2004 Mechanical characterization of heterogeneous soils with surface waves *Near Surf. Geophys.* **2** 249–58

Aki K 1970 Surface motion of a layered medium having an irregular interface due to incident plane SH waves *J. Geophys. Res.* **70** 933–54

Bard P Y 1995 Effects of surface geology on ground motion: recent results and remaining issues *Proc. 10th European Conf. on Earthquake Engineering (Vienna)* vol 1 (Rotterdam: Balkema) pp 305–23

Bard P Y and Bouchon M 1985 The two dimensional resonance of sediment-filled valleys *Bull Seismol. Soc. Am.* **75** 519–41

Cercato M 2009 Addressing non-uniqueness in linearized multichannel surface wave inversion *Geophys. Prospect.* **57** 27–47

Chavez-Garcia F, Rodriguez M, Field E and Hatzfeld D 1997 Topographic site effects. A comparison of two nonreference methods *Bull Seismol. Soc. Am.* **87** 591–604

Coduto D P 2001 *Foundation Design: Principles and Practices* (Englewood Cliffs, NJ: Prentice-Hall)

Dunkin J W 1965 Computation of modal solution in layered, elastic media at high frequencies *Bull Seismol. Soc. Am.* **12** 335–58

Foti S, Comina C, Boiero D and Socco L V 2008 Non-uniqueness in surface-wave inversion and consequences on seismic site response analyses *Soil Dyn. Earthq. Eng.* **29** 982–93

Huang Z X, Su W, Peng Y J, Zheng Y J and Li H Y 2003 Rayleigh wave tomography of China and adjacent regions *J. Geophys. Res.* **108** (B2) 2073

Idriss I M 1990 Response of soft soil sites during earthquakes *H B Seed Memorial Symp.* ed J M Duncan (Vancouver: BiTech Publishers) pp 273–89

Idriss I M and Seed H B 1969 Seismic response of horizontal soil layer *J. Soil Mech. Found. Div.* **95** 99–137

Idriss I M and Sun J I 1992 SHAKE91: a computer program for conducting equivalent linear seismic response analyses of horizontally layered soils deposits University of California, Davis, CA, USA

Keefe L 2005 *Earth Building: Methods and Materials, Repair and Conservation* (London: Taylor & Francis)

Keilis-Borok V I *et al* 1989 *Seismic Surface Waves in Laterally Inhomogeneous Earth* (Dordrecht: Kluwer)

Knopoff L 1972 Observation and inversion of surface wave dispersion *Tectonophysics* **13** 497–519

Konno K and Omachi T 1998 Ground motion characteristics estimated from spectral ratio between horizontal and vertical components of microtremors *Bull. Seismol. Soc. Am.* **88** 228–41

Lai C, Foti S and Rix G 2005 Propagation of data uncertainty in surface wave inversion *J. Environ. Eng. Geophys.* **10** 219–28

Lai C G and Wilmanski K 2005 *Surface Waves in Geomechanics: Direct and Inverse Modelling for Soils and Rocks* (Berlin: Springer)

Levshin A, Pisarenko V F and Pogrebinsky G A 1972 On a frequency–time analysis of oscillations *Ann. Geophys.* **28** 211–8

Lobkis O I and Weaver R L 2001 On the emergence of the Green's function in the correlations of a diffuse field *J. Acoust. Soc. Am.* **110** 3011–7

Louie J N 2001 Faster, better: shear-wave velocity to 100 meters depth from refraction microtremor arrays *Bull. Seismol. Soc. Am.* **91** 347–64

Matsumoto M and Nishimura T 1998 Mersenne twister: a 623-dimensionally equidistributed uniform pseudo-random number generator *ACM Trans. Model. Comput. Simul.* **8** 3–30

Moss E 2008 Quantifying measurement uncertainty of thirty-meter shear wave velocity *Bull. Seismol. Soc. Am.* **98** 1399–411

Mucciarelli M, Masi A, Gallipoli M R, Harabaglia P, Vona M, Ponzo F and Dolce M 2004 Analysis of RC building dynamic response and soil-building resonance based on data recorded during a damaging earthquake (Molise, Italy, 2002) *Bull. Seismol. Soc. Am.* **94** 1943–53

Nazarian S 1984 *In situ* determination of elastic moduli of soil deposits and pavement systems by spectral-analysis-of-surface waves method *PhD Thesis* University of Texas at Austin, TX, USA

Nazarian S, Stokoe K H II and Hudson W R 1983 Use of spectral analysis of surface waves method for determination of moduli and thicknesses of pavement systems *Transp. Res. Rec.* **930** 38–45

Nunziata C, Costa G, Natale M and Panza G F 1999 FTAN and SASW methods to evaluate Vs of neapolitan pyroclastic soils *Earthq. Geotech. Eng.* **1** 15–9

Pagliara G and Vignoli G 2006 Focusing inversion techniques applied to electrical resistance tomography in an experimental tank *Proc. IAMG'06*

Park C B, Miller R D and Xia J 1999 Multi-channel analysis of surface waves *Geophysics* **64** 800–8

Park C B, Miller R D, Xia J and Ivanov J 2007 Multichannel analysis of surface waves (MASW)—active and passive methods *The Leading Edge* January

Pritchett W C 1989 *Acquiring Better Seismic Data* (Dordrecht: Kluwer)

Rosenblad B L and Li J 2009 Performance of active and passive methods for measuring low-frequency surface wave dispersion curves *J. Geotech. Geoenviron. Eng.*. **135** 1419–28

Schnabel P B, Lysmer J and Seed H B 1972 SHAKE: a computer program for earthquake response analysis of horizontally layered sites *Report No EERC 72-12* Earthquake Engineering Research Center, University of California, Berkeley, CA, USA

Seed H B 1969 Influence of soil conditions on ground motion during earthquakes *J. Soil Mech. Found. Div.* **95** No SM1

Seed H B and Idriss I M 1970 Soil moduli and damping factors for dynamic response analyses *Report EERC 70-10* Earthquake Engineering Research Center, University of California, Berkeley, CA, USA

Seed H B, Wong R T, Idriss I M and Tokimatsu K 1986 Moduli and damping factors for dynamic analyses of cohesionless soils *J. Geotech. Eng.* **112** 1016–32

Socco L V and Boiero D 2008 Improved Monte Carlo inversion of surface wave data *Geophys. Prospect.* **56** 357–71

Socco L V, Boiero D, Comina C, Foti S and Wisén R 2008 Seismic characterization of an Alpine site *Near Surf. Geophys.* **6** 255–67

Socco L V and Strobbia C 2004 Surface wave methods for near-surface characterisation: a tutorial *Near Surf. Geophys.* **2** 165–85

Strobbia C and Cassiani G 2010 Refraction Microtremors (ReMi): data analysis and diagnostics of key hypotheses *Geophysics* at press

Strobbia C and Foti S 2006 Multi-offset phase analysis of surface wave data (MOPA) *J. Appl. Geophys.* **59** 300–13

Strobbia C L, Laake A, Vermeer P L and Glushchenko A 2009 Surface waves—use them then lose them *Proc. 71st EAGE Conf. & Exhibition*

Trampert J and Spetzler J 2006 Surface wave tomography: finite-frequency effects lost in the null space *Geophys. J. Int.* **164** 394–400

Vignoli G and Cassiani G 2009 Identification of lateral discontinuities via multi-offset phase analysis of surface wave data *Geophys. Prospect.* published online doi:10.1111/j.1365-2478.2009.00838.x

Vignoli G, Strobbia C, Cassiani G and Vermeer P 2010 Statistical multi-offset phase analysis for surface wave processing in laterally varying media *Geophysics* at press

Vignoli G and Zanzi L 2006 Focusing inversion technique applied to radar tomographic data http://arxiv.org/ftp/physics/papers/0606/0606243.pdf

Wathelet M 2005 Array recordings of ambient vibrations: surface-wave inversion *PhD Thesis* University of Liège, Belgium

Zhdanov M 2002 *Geophysical Inverse Theory and Regularization Problems* (Amsterdam: Elsevier)

Zhdanov M and Tolstaya E 2004 Minimum support nonlinear parametrization in the solution of a 3D magnetotelluric inverse problem *Inverse Probl.* **20** 937–52

Zhdanov M, Vignoli G and Ueda T 2006 Sharp boundary inversion in crosswell travel-time tomography *J. Geophys. Eng.* **3** 122–34

Zywicki D and Rix G J 1999 Frequency-wavenumber analysis of passive surface waves *Proc. Symp. on the Application of Geophysics to Environmental and Engineering Problems (Oakland, CA, USA)* pp 75–84